New Growth Mode through Decorated Twin Boundaries

Sebastian Bleikamp,[1,*] Arne Thoma,[1] Celia Polop,[1,†] Gerhard Pirug,[2] Udo Linke,[2] and Thomas Michely[1]

[1]*I. Physikalisches Institut, RWTH-Aachen University, 52056 Aachen, Germany*

[2]*Institut für Schichten und Grenzflächen, Forschungszentrum Jülich GmbH, 52425 Jülich, Germany*

(Received 12 December 2005; published 21 March 2006)

Scanning tunneling microscopy and low energy electron diffraction were used to investigate the growth of partly twinned Ir thin films on Ir(111). A transition from the expected layer-by-layer to a defect dominated growth mode with a fixed lateral length scale and increasing roughness is observed. During growth, the majority of the film is stably transformed to twinned stacking. This transition is initiated by the energetic avoidance of the formation of intrinsic stacking faults compared to two independent twin faults. The atomistic details of the defect kinetics are outlined.

DOI: 10.1103/PhysRevLett.96.115503 PACS numbers: 68.55.Ac, 61.14.Hg, 61.72.Mm, 61.72.Nn

It is well known that the properties of thin films depend crucially on their microstructure. One of the most important elements in thin film microstructure are stacking faults, which give rise to twin boundaries and twin crystallite formation [1]. Twin crystallites may critically influence the properties and functionality of films and devices (e.g., [2,3]). Understanding the mechanisms of stacking fault formation and the evolution of defects associated with their formation at atomic scale addresses thus one of the most serious problems in thin film growth. The dynamics of twin boundary motion, investigated recently for epitaxial films of a few layer thickness, highlighted the interdependence of twin boundaries and growth processes [4,5]. We choose a different approach here and follow the evolution of faulted Ir-films on Ir(111) in a large thickness range. As the system is homoepitaxial and should grow layer by layer in the absence of faults [6], the complex defect structures we observe evolving during growth display the machinery of kinetic processes triggered by the introduction of faults. We are able to identify the key mechanisms, which eventually drive the thin film into a new twin boundary growth mode: The formation of decoration defects at twin boundaries and the energetic avoidance of intrinsic stacking faults compared to two independent twins.

The experiments were performed in an UHV chamber with a base pressure $P < 5 \times 10^{-11}$ mbar. The sample was cleaned by repeated cycles of sputtering and annealing. Prior to deposition the sample was flashed to a temperature ensuring desorption of all species that might have adsorbed from the background gas. Ir was evaporated from a current heated Ir wire with a standard deposition rate of 1.3×10^{-2} ML/s, where 1 ML is the surface atomic density of the Ir(111) surface. Special care has been taken to ensure clean deposition conditions ($P < 1 \times 10^{-10}$ mbar). STM topographs are differentiated images and appear as if illuminated from the left.

Figure 1 shows the surface morphology after deposition of 1.05 to 70 ML Ir on Ir(111) at 350 K. After deposition of an amount of $\Theta = 1.05$ ML [Fig. 1(a)] the first layer is almost perfectly closed as in layer-by-layer growth. Indeed, layer-by-layer growth is expected for homoepitaxy on Ir(111) due to the absence of a step edge barrier [6]. However, on Ir(111) small mobile Ir clusters (dimers, trimers, etc.) occupy also faulted surface sites [7], which give rise to the homogeneous nucleation of fault islands [8]. Although at the beginning of deposition $\approx$12% of all islands formed were fault islands (compare Fig. 1 of [9]), most of the faulted island area is transformed to regular stacking upon close encounter of regular and faulted islands during layer completion through an atom-by-atom transfer from the faulted to the regular phase [9]. This self-healing mechanism comes only to rest if intersecting straight lines of fourfold-coordinated adsorption sites along $\langle 110 \rangle$ directions are formed [named *A* gaps, see Fig. 2(a)], which separate regular and faulted stacking. Upon subsequent deposition atoms are stably adsorbed into these fourfold-coordinated gap sites, thereby forming strings of monoatomic width [thin decoration rows, (tDR's)] which stabilize the phase boundary. The inset of Fig. 1(a) displays a triangular stacking fault area bounded by tDR's. On the large coalesced terrace of the first layer a new sequence of island nucleation has taken place and regular (triangular envelope pointing downwards) as well as faulted (triangular envelope pointing upwards) islands nucleated in the second layer.

In Fig. 1(b) with $\Theta = 5$ ML the STM topograph still indicates layer-by-layer growth. The fifth layer is nearly closed and islands of considerable size in the sixth layer are visible. A close inspection reveals now the presence of a large number of tDR's. They often terminate in grooves and islands are frequently attached to them. Their shape is influenced by the presence of tDR's and their shapes and sizes are extremely heterogeneous. Most noteworthy, somewhat fatter DR's (fDR's) are observed on top of islands [compare inset of Fig. 1(b)], thereby increasing the overall roughness of the morphology. After deposition of 20 ML [Fig. 1(c)] layer-by-layer growth is apparently lost. Stacked, elongated adatom islands oriented along the $\langle 110 \rangle$ directions are present at many locations. These

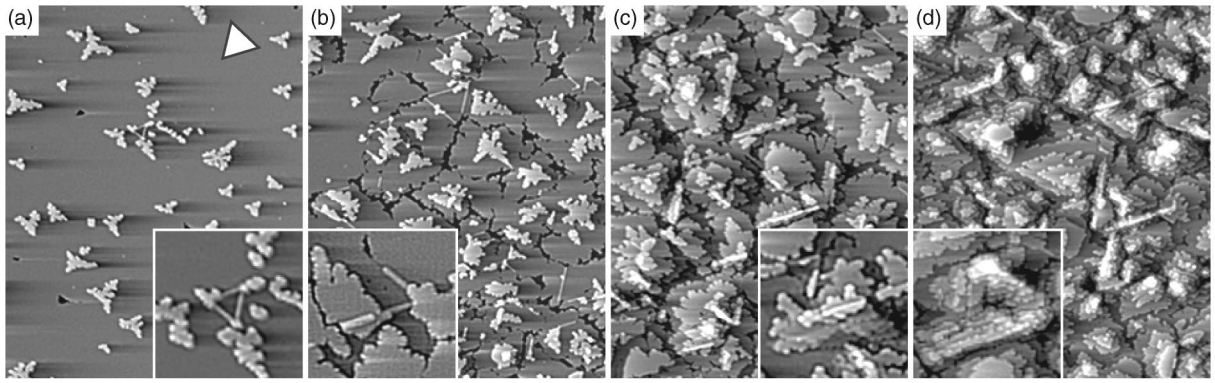

FIG. 1. STM topographs after deposition of (a) 1.05, (b) 5, (c) 20, and (d) 70 ML Ir on Ir(111) at 350 K. The triangle in (a) indicates the orientation of the triangular envelope of a faulted island. The image size is always 127 nm × 158 nm; insets are (a),(c) 25 nm × 25 nm and (b),(d) 18 nm × 18 nm.

mounds carry fDR's on their top from which material grows away [compare the inset of Fig. 1(c)]. Apparently an fDR acts as a preferential nucleation site for an adatom island and replicates itself on top of each such newly formed adatom island. A morphology of heterogeneous mounds is present in Fig. 1(d) with $\Theta = 70$ ML. Although the overall roughness is not large, it is clearly increasing with the deposited amount and even for the largest deposited amounts far from saturation. (For the range $\Theta \leq 90$ ML the analysis yields a power law behavior for the roughness increase with an exponent $\beta = 0.31 \pm 0.01$.) Upon close inspection, most mounds reveal the presence of DR-like defects, occasionally hardly visible due to small size or as one part of the boundary of the top layer island. Interestingly, although many fDR's are present, no more tDR's can be found.

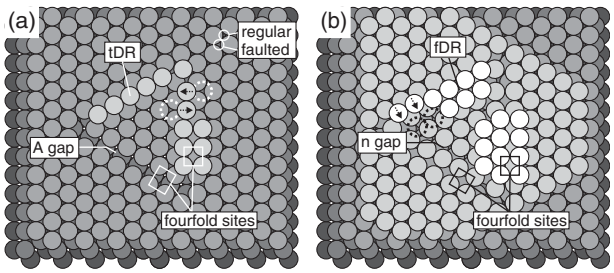

FIG. 2. (a) Ball model displaying a triangular stacking fault area surrounded by A gaps. The fourfold-coordinated adsorption sites offered by the A gaps are partly filled by atoms forming tDR's. Attachment of an atom at one of the locations indicated by the dashed circles causes a tDR atom to relax slightly away from its fourfold-coordinated adsorption site, either inward or outward. Inward relaxation of a tDR by a few atoms attached at the outside of the triangle is shown. Thereby new fourfold adsorption sites are created in the next higher layer. (b) Situation in the next higher layer. If the inner area is filled with atoms, a narrow gap (n gap) between the tDR and the next row of atoms is formed. A fDR is created by occupying sites on the n gap (dashed circles) next to a tDR and the inward relaxation of the tDR. Attaching further atoms leads to new fourfold sites.

Unlike for many other homoepitaxial growth systems, inspection of Fig. 1 indicates no or very little coarsening. The quantitative analysis of the evolution of the lateral length scale is based on the height-height correlation function $G(\vec{r})$ for representative topographs [10,11]. Here we used as a measure for the average length scale $\lambda = 8\omega$ with ω being the width at half maximum of the radially averaged $G(r) = \langle G(\vec{r})\rangle_{|\vec{r}|=r}$, i.e., $G(\omega) = 1/2G(0)$. In the radially averaged power spectral densities for deposited amounts larger than 20 ML a single peak develops indicating the dominant wavelength in the morphology and is thus another estimate for λ. As visible in Fig. 3 after some initial scatter (related to the phase of growth in the layer-by-layer regime) around 10 ML a fixed length scale of about 40 nm establishes. For the same $\Theta \approx 10$ ML also the decoration row density reaches a saturation value. In Fig. 3 the square root of the inverse decoration row density—the average decoration row separation d_R—is plotted. The remarkable coincidence of the saturation of λ and d_R, as

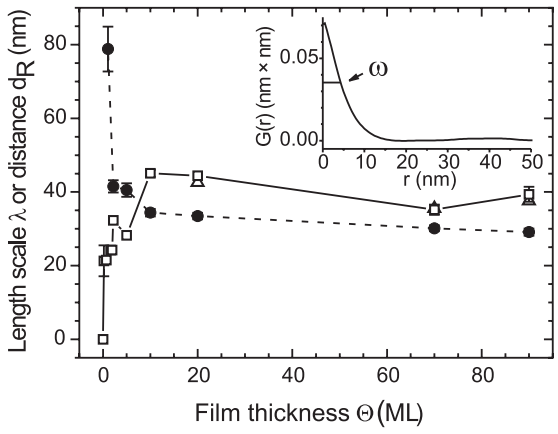

FIG. 3. Average lateral length scale $\lambda = 8\omega$ as obtained from $G(r)$ (open squares) and from the radially averaged power spectral density (for $\Theta \geq 20$ ML, open triangles) as well as the average distance of decoration rows d_R (full circles) as a function of Θ. Lines are to guide the eye. Inset: $G(r)$ of a typical image with $\Theta = 70$ ML.

well as their rough agreement in their saturation magnitude, are strong hints for a link between these two quantities. With the observation of Fig. 1 that eventually most mounds contain a DR, this link is evident. Structure formation is dominated by the presence of DR's. Indeed, they are sites of heterogeneous nucleation for adatom islands, thereby eliminating homogeneous island nucleation together with layer-by-layer growth. The discussion how this works in atomic detail is postponed until the twinned surface area in the thin films is analyzed.

The stacking sequence in a thin film is not directly accessible to STM. For coverages up to 5 ML, the surface areas with a buried fault plane—the twinned surface areas—may be identified by STM as areas surrounded by tDR's. Up to this thickness range, the fraction of twinned surface area exhibits an oscillatory behavior with minima for the full ML due to self-healing. The level of these minima increases from 1.5% at 1 ML over 4.3% at 2 ML to $\approx 30\%$ at 5 ML. Beyond 5 ML, the direct STM method fails. Low energy electron diffraction (LEED) is used to determine the twinned surface fraction. LEED of a clean Ir(111) single crystal exhibits at 235 eV electron energy bright (10) and darker (01) spots [compare Fig. 4(a)]. The I/V curves of the two spot types are very different. The LEED patterns and the I/V curves of an entirely twinned thin film correspond to the ones of a single crystal rotated by 180° around the surface normal. Thus, to first approximation, the I/V curves of the (10) and (01) spots of a partly twinned thin film (with domains of sufficient size) can be obtained as linear combinations of the I/V curves of the (10) and (01) spots of an unrotated and rotated perfect crystal. The LEED pattern in Fig. 4(b) after deposition of 70 ML exhibits now brighter (01) than (10) spots. This shows immediately that the majority of the surface area is twinned. Fitting both resulting I/V curves by linear combinations with the same two coefficients, a twinned surface area of $(56.3 \pm 0.4)\%$ is obtained. For the larger amount of 90 ML an even larger twinned fraction of $(62.0 \pm 0.7)\%$ results. Isochronal annealing for intervals of 180 s in temperature steps of 100 K exhibits only above 1000 K a gradual reduction of the twinned surface fraction. For the 90 ML film after annealing to 1025 K, the twinned surface area is still above 60%. For such annealed films the STM variant of the postdecoration method of Meinel *et al.* [12] was used, yielding for the twinned surface fraction quantitative agreement with our LEED results.

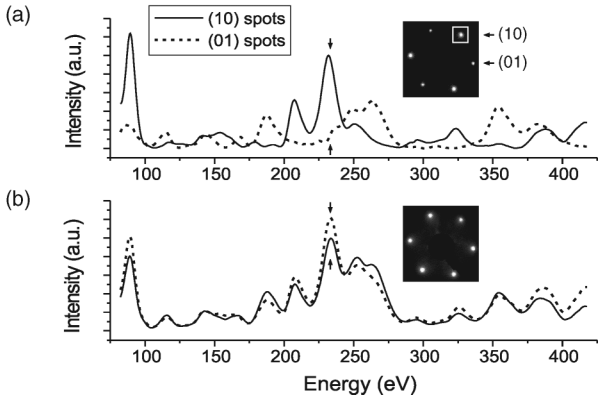

FIG. 4. LEED patterns and I/V curves of (a) the Ir(111) single crystal and (b) after deposition of 70 ML Ir on Ir(111). LEED patterns are recorded at 235 eV; this energy is indicated by arrows in the I/V spectra. Straight lines: (10) spots, dashed lines: (01) spots. Intensities are spatially integrated over windows around the spots and averaged over the three equivalent spots. Window size is indicated by the rectangle in the inset.

In a toy model for twinning we assume a fixed, layer independent, stacking fault probability P_{SF} during thin film growth. For simplicity it is assumed to be identical to the fraction of the area changing its character (from regular to twinned or from twinned to regular). Then, in the layer $N+1$ the area of regular stacking $A_{N+1,\mathrm{reg}}$ and the twinned area $A_{N+1,\mathrm{twin}}$ are:

$$A_{N+1,\mathrm{twin}} = P_{\mathrm{SF}} A_{N,\mathrm{reg}} + (1 - P_{\mathrm{SF}}) A_{N,\mathrm{twin}}, \quad (1)$$

$$A_{N+1,\mathrm{reg}} = (1 - P_{\mathrm{SF}}) A_{N,\mathrm{reg}} + P_{\mathrm{SF}} A_{N,\mathrm{twin}}. \quad (2)$$

Independent of the starting conditions and for nonzero P_{SF}, this model yields equal amounts of twinned and regular surface area for sufficiently large N. As this contradicts our experimental results, apparently there must be some correlation between the introduction of stacking faults in different layers.

A key to understand how the twinned surface area may become so large may be found in Fig. 5. Figure 5(a) displays a STM topograph of a stacking fault area with DR's, which is analyzed in Figs. 5(b) and 5(c). In the layer below the island level, a triangular stacking fault area bounded by tDR's had been formed during growth [see also Fig. 2(a)]. Compared to the terrace, the tDR's offer sites of larger

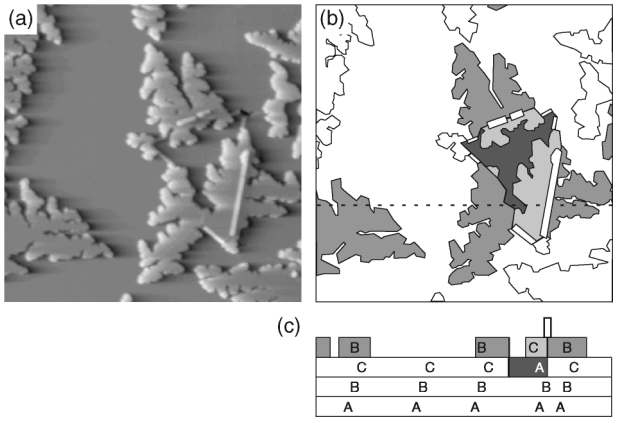

FIG. 5. (a) STM topograph of a stacking fault area with decoration rows. Image size 56 nm × 56 nm. (b) Schematic drawing of the situation of (a). Shading according to the stacking sequence [see (c)]. All areas other than white are the twinned surface area with a single buried stacking fault. (c) Cross section of (b) along the dotted line. Labeling of the layers with A, B, and C indicates the stacking sequence in the usual notation (compare, e.g., [13]). See also, text.

coordination and thus are binding sites for the attachment of additional atoms. In consequence, and as visible in Fig. 5(a), heterogeneous nucleation of island branches took place at the tDR's. Attachment of atoms and subsequent growth will cause the positions of the fourfold-coordinated tDR atoms to relax a little from their ideal positions. As indicated by the arrows in Fig. 2(a), a tDR atom may in principle relax in both directions normal to the tDR. If the tDR's relax outwards, an intrinsic stacking fault (two faults on subsequent planes) is formed *inside* the triangular area, while no fault is induced outside of it. As two faults cancel each other, without additional faults in subsequent growth the area would be detected as regular. If the tdR's relax inwards, toward the center of the triangular faulted area, *outside* new stacking faults are induced, while inside no new fault is formed. If no additional faults are placed during subsequent growth, the triangular area *and* its surrounding would be detected as twinned.

We analyzed many situations similar to the one depicted in Fig. 5 and invariably find that the latter situation is realized; i.e., no intrinsic faults are formed. This may be concluded with certainty from the analysis of the preferential growth directions of the islands growing away from the tDR's. For example, the islands which heterogeneously nucleated at the tDR's of the central faulted area in Fig. 5(a) exhibit only growth directions characteristic for faulted growth [compare with the triangle in Fig. 1(a)]. Density functional theory calculations [13] for faults on Ir(111) net planes yield 0.086 eV/atom for a single fault (a twin), but 0.112 eV/atom to form a second fault immediately above an existing one, i.e., to complete the formation of an intrinsic fault. In the presence of sufficient mobility of atoms attaching to tDR's, it is this energy difference of about 0.026 eV/atom which causes the avoidance of intrinsic faults and the preference for the creation of new faults outside the already faulted triangular area. Thus tDR's couple fault probabilities in two layers, prevent cancellation of existing faults by second ones and cause rapid lateral fault proliferation.

The effect of tDR's alone, however, would neither be sufficient to explain the observed growth mode nor the transformation of the majority of the film to twinned stacking. There are two more effects to consider: (i) An initial tDR gives rise to the formation of an fDR in the layer above, which replicates itself over and over again in higher layers. (ii) These fDR's prevent the introduction of further stacking faults adjacent to their both sides. The self-replication of DR's is based on the fact that a DR always induces the formation of fourfold-coordinated, ''sticky'' sites one layer above. Figure 2(b) depicts the transition from tDR's to fDR's. After the tDR has been incorporated into the layer, there are two adjacent rows of preferred adsorption sites: the fourfold-coordinated ones and next to them those which are above the narrow gap in the layer below. Growth causes, therefore, first the formation of a new decoration row of double atomic width or fDR (as also visible in Fig. 5(a) *on* the central island structure) and then subsequent attachment of atoms to both sides (i.e., heterogeneous island nucleation and growth). The attachment on both sides of the fDR is only possible on regular sites [see Fig. 2(b)] and induces the new formation of fourfold adsorption sites [see Fig. 2(b)] for atoms of the next higher layer which in turn initiates again decoration row formation (and so forth).

The self-replication of the DR's [effect (i)] together with their ability to trigger heterogeneous nucleation explain the coupling of d_R and λ, the breakdown of layer-by-layer growth and the mounds with the DR's on their top terrace. The suppression of fault cancellation [effect (ii)] after a fault bounded by tDR's has been formed and proliferated into its surroundings explains how the majority of the film surface area may appear twinned after sufficiently long deposition.

In conclusion, we observed a transition from layer-by-layer growth to a defect dominated growth with a fixed length scale in homoepitaxy on Ir(111). During this transition, the majority of the surface area becomes twinned. At the beginning of this transition, the formation of thin, monatomic decorations rows on the phase boundary between regular and faulted surface areas takes place. Next, the energetic avoidance of the formation of intrinsic stacking faults causes the spread of these initial fault areas into their surroundings. Replication of decoration rows in higher layers acting as nucleation centers and suppression of new fault formation next to them completes this transition.

Support by the Deutsche Forschungsmeinschaft through the project ''Kinetics of Stacking Faults in Thin Films'' is acknowledged.

*Electronic address: bleikamp@physik.rwth-aachen.de
†Present address: Department Física de la Materia Condensada, Universidad Autónoma de Madrid, 28049 Madrid, Spain.

[1] M. J. Stowell, in *Epitaxial Growth*, edited by J. W. Matthews (Academic, New York, 1975), Part B, p. 437.
[2] S. Ha *et al.*, Phys. Rev. Lett. **92**, 175504 (2004).
[3] E. Valcheva *et al.*, J. Phys. Condens. Matter **14**, 13 269 (2002).
[4] F. El Gabaly *et al.*, Science **308**, 1303 (2005).
[5] W. L. Ling *et al.*, Phys. Rev. Lett. **95**, 166105 (2005).
[6] S. C. Wang and G. Ehrlich, Phys. Rev. Lett. **67**, 2509 (1991).
[7] S. C. Wang and G. Ehrlich, Surf. Sci. **239**, 301 (1990).
[8] C. Busse *et al.*, Phys. Rev. Lett. **91**, 056103 (2003).
[9] C. Busse and T. Michely, Surf. Sci. **552**, 281 (2004).
[10] M. Rost *et al.*, Surf. Sci. **369**, 393 (1996).
[11] WSxM©; http://www.nanotec.es.
[12] K. Meinel *et al.*, Phys. Status Solidi A **110**, 189 (1988).
[13] N. M. Rosengaard and H. L. Skriver, Phys. Rev. B **47**, 12 865 (1993).